

This discussion paper is/has been under review for the journal Hydrology and Earth System Sciences (HESS). Please refer to the corresponding final paper in HESS if available.

# Bench scale laboratory tests to analyze non-linear flow in fractured media

**C. Cherubini, C. I. Giasi, and N. Pastore**

Sezione di Ingegneria Geotecnica e Geoambientale – DIAC,  
Politecnico di Bari, Via Orabona 4, 70100 Bari, Italy

Received: 29 March 2012 – Accepted: 14 April 2012 – Published: 25 April 2012

Correspondence to: C. Cherubini (claudia.cherubini@gmail.com)

Published by Copernicus Publications on behalf of the European Geosciences Union.

**HESSD**

9, 5575–5609, 2012

**Bench scale  
laboratory tests**

C. Cherubini et al.

Title Page

Abstract

Introduction

Conclusions

References

Tables

Figures

◀

▶

◀

▶

Back

Close

Full Screen / Esc

Printer-friendly Version

Interactive Discussion



## Abstract

The knowledge of flow phenomena in fractured rocks is very important for groundwater resources management in hydrogeologic engineering.

A critical emerging issue for fractured aquifers is the validity of the Darcian-type “local cubic law” which assumes a linear relationship between flow rate and pressure gradient to accurately describe flow patterns.

Experimental data obtained under controlled conditions such as in a laboratory allow to increase the understanding of the fundamental physics of fracture flow and to investigate the presence of non linear flow inside the fractures which brings to substantial deviation from Darcy’s law.

In this study the presence of non linear flow in a fractured rock formation has been analyzed at bench scale in laboratory tests. The effects of non linearity in flow have been investigated by analyzing hydraulic tests on artificially created fractured rock samples of parallelepiped ( $0.60 \times 0.40 \times 0.8\text{m}$ ) shape.

The volumes of water passing through different paths across the fractured sample for various hydraulic head differences have been measured, and the results of the experiments have been reported as flow rate/specific discharge vs. head gradient. The experimental results closely match the Forchheimer equation and describe a strong inertial regime. Successively the results of the test have been interpreted by means of numerical simulations. For each pair of ports several steady-state simulations have been carried out varying the hydraulic head difference between inlet and outlet ports. The estimated linear and non linear Forchheimer coefficients have been correlated to each other and, respectively to the tortuosity of the flow paths. A correlation among the linear and non linear Forchheimer coefficients is evident. Moreover, a tortuosity factor has been determined that influences flow dynamics.

# HESSD

9, 5575–5609, 2012

## Bench scale laboratory tests

C. Cherubini et al.

Title Page

Abstract

Introduction

Conclusions

References

Tables

Figures

◀

▶

◀

▶

Back

Close

Full Screen / Esc

Printer-friendly Version

Interactive Discussion



# 1 Introduction

The aim of present work is to experimentally investigate the behavior of high velocity flow regime in fractured network at bench scale.

High velocity flow dynamics can have significant impact in diverse fields such as radioactive waste disposal, geothermal engineering, environmental risk assessment and remediation, reservoir engineering, and groundwater hydrology (Cherubini et al., 2010).

In most studies examining hydrodynamic processes in saturated porous and fractured media, it is assumed that flow is described by the Darcy's law which expresses a linear relationship between pressure gradient and flow rate. Darcy's law has been demonstrated to be valid low flow regime ( $Re \ll 1$ ). For  $Re > 1$  a non linear flow behavior is likely to occur.

Ing and Xiaoyan (2002) have showed how non-Darcian flow has a significant impact on consolidation rate in geotechnics.

Basak and Rajagopalan (1982) have demonstrated that seawater intrusion length increases when the flow deviates from Darcian linearity.

As far as solute transport, non-Darcian flow might give rise to tailing in contaminant's breakthrough curves that show a non-Fickian behavior (Boutt et al., 2006; Cardenas et al., 2007).

Moreover, exposure and risk assessment of chemical pollution based on the applicability of Darcy's law are sometimes inappropriate when applied to fractured aquifers because of the possible occurrence of nonlaminar flow regime. In fact, considerable evidence exists to refute their reliability in assessing solute-migration rates and for determining downgradient concentrations (Field, 1997).

The mathematical representation of fluid dynamics in fractured rock aquifers is of a great concern for environmental and petroleum engineering and in geological sciences.

## Bench scale laboratory tests

C. Cherubini et al.

Title Page

Abstract

Introduction

Conclusions

References

Tables

Figures

◀

▶

◀

▶

Back

Close

Full Screen / Esc

Printer-friendly Version

Interactive Discussion



The local Cubic Law adapts Darcy's law to flow through fractures under the assumption of ideal fractures with flat and smooth and parallel walls and infinite lengths, together with laminar flow, incompressible fluid and confined aquifer configuration.

Real rock fractures instead, are characterized by rough walls, variable surfaces and geometry and apertures. The presence of asperities and obstructions or sharp changes in fracture profile is the reason for microscopic inertial phenomena that cause an extra macroscopic pressure loss which deviates flow from linearity.

Roughness has a large influence in fluid flow and transport through tight, rough-walled fractures, (Boutt et al., 2006) where non-Darcian flow is particularly easy to occur (e.g. Lomize, 1951; Louis, 1969; Qian et al., 2005, 2007, 2010; Wen et al., 2006).

Flow regimes and non-linear behavior of fluid flow through fractures have been investigated, empirically (Lomize, 1951; Louis, 1969), experimentally (Witherspoon et al., 1980; Qian et al., 2005; Chin et al., 2009), and numerically (Zimmerman et al., 2004; Kolditz, 2001; Brush and Thomson, 2003).

Zimmerman et al. (2004) studied non-linear flow regimes both with experimental and numerical simulation of Navier-Stokes equations and suggested the critical Reynolds number of 10 for practical purposes.

Witherspoon et al. (1980) conducted experiments in rock fractures to study the hydraulic behavior. They demonstrated that if fractures are rough or flow velocities are high, Darcy's law is not applicable.

Chin et al. (2009) investigated the variation of effective hydraulic conductivity as a function of specific discharge in several 0.2-m and 0.3-m cubes of Key Largo Limestone. The experimental results closely match the Forchheimer equation.

Qian et al. (2005) carried out laboratory experiments to study groundwater flow in a single fracture under different conditions of fracture aperture, surface roughness, and water pressure. The experimental results show that the average flow velocity ( $V$ ) could be approximated by an empirical exponential function of the hydraulic gradient ( $I$ ), which varies in the range of 0.003–0.02. The power index of the exponential function is

## Bench scale laboratory tests

C. Cherubini et al.

Title Page

Abstract

Introduction

Conclusions

References

Tables

Figures

◀

▶

◀

▶

Back

Close

Full Screen / Esc

Printer-friendly Version

Interactive Discussion



close to 0.5. Such a  $V^{-1}$  relationship indicates a non-Darcian turbulent flow even though the Reynolds number is relatively low.

Javadi et al. (2010) performed both laminar and turbulent flow simulations for a wide range of flow rates in an artificial three-dimensional fracture. They developed a new geometrical model for non-linear fluid flow through rough fractures, which suggests a polynomial expression, like Forchheimer's law, to describe the dependence of pressure drop on flow rate. Finally, this model has been evaluated with experimental results of a fracture with different geometries. A good accuracy was found between the proposed model and turbulent flow simulation results.

Brush and Thomson (2003) carried out simulations of fluid flow through single rough-walled fractures with various apertures using Navier-Stokes, Stokes, and Local Cubic Law simulations. They observed that several Navier-Stokes velocity profiles have flatter peaks or noses that indicate the formation of an inertial core between the walls. They demonstrated that inertial forces can significantly influence the internal flow field within a fracture so that the forces driving the flow field are reduced and the overall flow rate is decreased. As the mean aperture increases, the effect of surface roughness diminishes (Boutt et al., 2006).

Louis (1984) empirically defined five steady-state flow regimes, from smooth laminar to fully developed turbulent, depending on various degrees of relative roughness, fracture aperture, hydraulic head gradient in the fracture plane and kinematic viscosity.

Fully developed turbulent flow conditions are more likely to occur when velocities are high, i.e. in karstic conduits, whereas, in presence of lower velocities, non-linear laminar flow happens when inertial effects become important, e.g. due to roughness, restrictions, presence of contact points between the fracture walls and non-rectilinear profile.

Differently from conduits, the flow regime prevailing between rough-walled surfaces does not immediately switch from Darcy flow to turbulent flow as velocity is increased or viceversa (Kohl at al., 1997) but transitional regimes can be distinguished.

## Bench scale laboratory tests

C. Cherubini et al.

Title Page

Abstract

Introduction

Conclusions

References

Tables

Figures

◀

▶

◀

▶

Back

Close

Full Screen / Esc

Printer-friendly Version

Interactive Discussion



On the basis of a recent classification of Skjetne (1995), three different principal flow regimes can be distinguished: (1) linear laminar flow, (2) nonlinear rough laminar flow (weak or strong inertia) and (3) turbulent flow.

A fracture can be envisioned as two rough surfaces in contact. Cross sectional solid areas representing asperities in contact are similar to the grains of porous media. It is therefore possible to apply the general equations describing flow and transport in porous as well as in fractured media. One element to take into account is that the void space of the fracture is interconnected in one surface, so the fracture is best described as a two-dimensional porous medium (National Research Council, 1996).

In literature are reported different laws that account for the non linear relation between velocity and pressure gradient.

The weak inertia equation is a cubic extension of Darcy's law and describes pressure loss vs. flow rate for low flow rates:

$$-\nabla p = \frac{\mu}{k} \cdot \mathbf{v} + \frac{\gamma \rho^2}{\mu} \cdot \mathbf{v}^3 \quad (1)$$

Where  $p$  ( $\text{ML}^{-1}\text{T}^{-2}$ ) is the pressure,  $k$  ( $\text{L}^2$ ) is the permeability,  $\mu$  ( $\text{ML}^{-1}\text{T}^{-1}$ ) is the viscosity,  $\rho$  ( $\text{ML}^{-3}$ ) is the density,  $\mathbf{v}$  ( $\text{LT}^{-1}$ ) is the velocity and  $\gamma$  (L) is called the weak inertia factor.

This law was first shown numerically (Barrère, 1990), and then derived theoretically for homogeneous isotropic media (Mei and Auriault, 1991).

In case of higher Reynolds numbers ( $Re \gg 1$ ) the pressure losses pass from a weak inertial to a strong inertial regime, described by the Forchheimer equation (Forchheimer, 1930), given by:

$$-\nabla p = \frac{\mu}{k} \cdot \mathbf{v} + \rho \beta \cdot \mathbf{v}^2 \quad (2)$$

Where  $\beta$  is called the inertial resistance (coefficient), or non-Darcy coefficient.

## Bench scale laboratory tests

C. Cherubini et al.

Title Page

Abstract

Introduction

Conclusions

References

Tables

Figures

◀

▶

◀

▶

Back

Close

Full Screen / Esc

Printer-friendly Version

Interactive Discussion



Forchheimer proposes a further expression in which the pressure gradient can be described by a third order polynomial, whereas Hassanizadeh and Gray (1987) propose an extension that includes the effects of a transient flow regime.

Another commonly used non-Darcian flow equation is the Izbash or power-law equation (Izbash, 1931):

$$-\nabla p = \lambda \cdot v^n \quad (3)$$

Where  $\lambda$  and  $n$  are two constant coefficients and  $1 \leq n \leq 2$ : If  $n = 1$  the flow is Darcian, whereas if  $n = 2$  the flow is fully developed turbulent. The Forchheimer and Izbash equations are equivalent when the linear term in the Forchheimer equation is equal to zero and  $n = 2$ .

The Forchheimer equation can be considered as an expansion of the linear Darcy's law because it includes both the viscous and inertial effects.

On the other side, power law functions such as the Izbash equations are more appropriate to model post-linear non-Darcian flows that might be caused predominately by turbulent effects (Wen et al., 2008).

Experimental evidence has shown that both the Forchheimer and the Izbash equations are equally possible, depending on field-specific conditions (Wen et al., 2006).

A general Darcian-like relationship can be used (Chin et al., 2009) to describe all the mentioned flow regimes and to account for nonlinearities in the relationship between hydraulic head gradient and flow velocity:

$$v = -K_{\text{eff}}(\nabla h) \cdot \nabla h \quad (4)$$

$K_{\text{eff}}$  ( $\text{LT}^{-1}$ ) is the effective hydraulic conductivity, respectively, and  $h = p/\rho g$  (L) is the total hydraulic head. For instance, according to Forchheimer's law, effective hydraulic conductivity can be written as (Cakmak, 2009):

$$K_{\text{eff}} = \frac{2}{a + \sqrt{a^2 + 4b\|\nabla h\|}} \quad (5)$$

**Bench scale laboratory tests**

C. Cherubini et al.

Title Page

Abstract Introduction

Conclusions References

Tables Figures

◀ ▶

◀ ▶

Back Close

Full Screen / Esc

Printer-friendly Version

Interactive Discussion



Where  $a$  ( $\text{TL}^{-1}$ ) and  $b$  ( $\text{T}^2\text{L}^{-2}$ ) are the linear and inertial coefficients, respectively in terms of hydraulic head and can be expressed accordingly to previous expressions as:

$$a = \frac{\mu}{\rho g k}; \quad b = \frac{\beta}{g} \quad (6)$$

5 In same way for a discontinuity can be defined the effective fracture transmissivity and the relationship between specific discharge  $q$  ( $\text{L}^2\text{T}^{-1}$ ) and hydraulic head gradient can be written as:

$$\mathbf{q} = \frac{2}{a_f + \sqrt{a_f^2 + 4b_f\|\nabla h\|}} \nabla h \quad (7)$$

$a_f$  and  $b_f$  are related to  $a$  and  $b$ :

$$10 \quad a_f = \frac{a}{w}; \quad b_f = \frac{b}{w^2} \quad (8)$$

where  $w$  represents the aperture of fracture.

In the present paper, several fracture network configurations are studied in order to observe non-linear behavior of flow regime. The study is aimed at determining the relationship between the average velocity and the hydraulic gradient and will serve as first step exploration of further investigation of solute transport in fracture systems under the non-Darcian flow.

## 2 Experimental setup

### 2.1 Characterization and preparation of block sample

20 The experiments have been performed on a limestone block with parallelepiped shape ( $0.6 \times 0.4 \times 0.08 \text{ m}^3$ ) recovered from the “Calcarea di Altamura” formation which is located in Apulia region in south-eastern part of Italy.

Title Page

Abstract

Introduction

Conclusions

References

Tables

Figures

◀

▶

◀

▶

Back

Close

Full Screen / Esc

Printer-friendly Version

Interactive Discussion



---

**Bench scale  
laboratory tests**
C. Cherubini et al.

---

[Title Page](#)[Abstract](#)[Introduction](#)[Conclusions](#)[References](#)[Tables](#)[Figures](#)[◀](#)[▶](#)[◀](#)[▶](#)[Back](#)[Close](#)[Full Screen / Esc](#)[Printer-friendly Version](#)[Interactive Discussion](#)

In Table 1 are reported the bulk hydraulic parameters of limestone block. The fracture network has been made artificially through 5 kg mallet blows. The fissured system and the fracture aperture on the block surfaces have been recorded with high resolution digital camera. Subsequently the images have been scaled and rectified using *Perspective Rectifier* (www.rectifiersoft.com) (Fig. 1). Profiles of discontinuities and aperture measurements have been extracted from the recorded images using *edge* function with “*canny*” filter built-in *Scilab Image Processing Toolbox* (www.scilab.org). For each discontinuity, the median profile, aperture distribution and the fractal dimension using box counting method have been determined (Table 2).

The surface of block sample has been sealed with transparent epoxy resin (Leven et al., 2004). A hole of 1 cm diameter has been opened for each discontinuity in correspondence of the boundary of the block.

The spatial position of opened ports (Fig. 2) and the illustration of construction details (Fig. 3) have been reported.

## 2.2 Materials and methods

In Fig. 4 is shown the diagram of experimental set up. The sealed block sample is connected with a hydraulic circuit. Water moves from the upstream to the downstream tank and returns to the upstream tank by means of a transfer pump. A flow cell is connected to the outlet port. The sealed block and the tubes of hydraulic circuits are completely saturated. Initially, the valves “*a*” and “*b*” are closed and the hydrostatic head in flow cell is equal to  $h_0$ . The ultrasonic flow velocimeter measures the snapshot flow rates that enter the sealed block. The experiment begins with the opening of the valve “*a*” and it is reclosed when the hydraulic head in the flow cell is equal to  $h_1$ . Finally the hydraulic head in the flow cell is reported to  $h_0$  through the opening of the valve “*b*”.

The average flow rate through the sealed block can be estimated by means of the volumetric method:

$$\bar{Q} = \frac{A_1}{t_1 - t_0} (h_1 - h_0) \quad (9)$$

During the experiments, these values are compared with the snapshot flow rates measured by ultrasonic velocimeter in order to check the absence of hydraulic loss due to obstructions and leaks in the hydraulic system.

The experiment is repeated changing the hydraulic head  $h_c$  of the upstream tank and for each configuration of inlet-outlet ports. For different values of  $h_c$  the time  $\Delta t = (t_1 - t_0)$  required to fill the flow cell from  $h_0$  to  $h_1$  has been registered.

The storage property of the upstream tank is much greater than downstream flow cell ( $A_1 \gg A_2$ ) therefore during the experiment the upstream hydraulic head can be considered constant. Given that the sealed block sample and the hydraulic circuit are very rigid, their compressibility can be neglected.

On the basis of these assumptions the drainage process is governed by the following equation:

$$A_1 \frac{dh}{dt} = \Gamma(\Delta h)(h_c - h) \quad (10)$$

Where:  $A_1$  ( $L^2$ ) is the section area of the flow cell;  $h$  (L) is the hydraulic head of the downstream flow cell;  $h_c$  (L) is the hydraulic head of upstream tank;  $\Gamma(\Delta h)$  ( $L^2 T^{-1}$ ) is the hydraulic conductance term (Harbough, 2005) representative of both hydraulic circuit and the active fracture network configuration.

Hydraulic loss within the single hydraulic circuit can be expressed according to Chezy's law as:

$$Q = C \sqrt{|\Delta h|} \Rightarrow \Delta h = \frac{1}{C^2} Q^2 \quad (11)$$

Where  $C$  is a characteristic coefficient related to the roughness, section and length of the tubes of the hydraulic circuit.

Whereas, only for the sealed block,  $\Delta h - Q$  relationship can be represented through the following polynomial expression:

$$\Delta h = A \cdot Q + B \cdot Q^2 \quad (12)$$

**Bench scale laboratory tests**

C. Cherubini et al.

Title Page	
Abstract	Introduction
Conclusions	References
Tables	Figures
◀	▶
◀	▶
Back	Close
Full Screen / Esc	
Printer-friendly Version	
Interactive Discussion	



Where  $A$  and  $B$  are the linear and non-linear hydraulic loss coefficients, respectively and are related to the roughness, aperture, lengths and shape of fractures.

Combining Eqs. (11) and (12) the conductance term representative of the whole hydraulic system assumes the following expression:

$$\Gamma(\Delta h) = \frac{2}{A + \sqrt{A^2 + 4(B + C^{-2})|\Delta h|}} \quad (13)$$

Substituting Eq. (13) in Eq. (10) and integrating the latter from  $t = t_0$  to  $t = t_1$  with the initial condition  $h = h_0$  the following equation is obtained:

$$A_1 \left( -\sqrt{A^2 + 4(B + C^{-2})(h_c - h)} - A \ln \left( \sqrt{A^2 + 4(B + C^{-2})(h_c - h)} - A \right) \right) \Big|_{h_0}^{h_1} = t_1 - t_0 \quad (14)$$

Then, fitting experimental relationship between the time  $\Delta t = (t_1 - t_0)$  and hydraulic head of downstream tank  $h_c$ , an estimate of parameter  $A$ ,  $B$  and  $C$  can be made. Parameter  $C$  is estimated conducting the mentioned experiments without the sealed block ( $A = 0$ ;  $B = 0$ ).

### 3 Experimental results

Several experiments have been conducted for each in-out port configurations. Control head  $h_c$  varies in the range of 0.17–1.37 m and the average flow rates observed is in the range of  $3.08 \times 10^{-7}$ – $2.99 \times 10^{-5} \text{ m}^3 \text{ s}^{-1}$ . All the experiments carried out show a non-linear  $Q - \Delta h$  relationship that can be well described by Eq. (12). Figure 5 shows the fitting method described in previous section to estimate the linear ( $A$ ) and non-linear ( $B$ ) terms. The double entry Table 3 show the estimated of  $A$  and  $B$  for each pair of ports.

Title Page

Abstract

Introduction

Conclusions

References

Tables

Figures

◀

▶

◀

▶

Back

Close

Full Screen / Esc

Printer-friendly Version

Interactive Discussion



If the experiments were carried out on a single fracture,  $a_f$  and  $b_f$  coefficients of Forchheimer Eq. (5) could be derived in analytical way from Eq. (12). In the present case, in order to obtain Forchheimer term a numerical model has been implemented.

Starting from fracture profiles (Fig. 1) three-dimensional geometry of fissured system has been carried out using *GMSH* pre-processing tool (Geuzaine and Remacle, 2010). Geometry has been imported in *Comsol Multiphysics*<sup>®</sup> v4.0a (Comsol AB, 2010) using STL exchange file format (Vinciguerra and Bernabè, 2010). Furthermore the geometry of the hole of ports has been modeled. Figure 7a shows the geometry of the fissured system and of the port holes. COMSOL uses the finite element scheme to solve generic partial differential equations. In particular manner “*Weak Form Boundary PDE Interfaces*” included in “*Mathematics Module*” has been used.

For each pair of ports several steady-state simulations have been conducted varying the hydraulic head difference between inlet and outlet ports (Fig. 7b). For each configuration ports and for each numerical simulation the flow rate obtained from Eq. (9) ( $Q_{obs}$ ) and from the numerical model ( $Q_{sim}$ ) in correspondence of outlet port have been compared. The idea is to find the parameters  $a_f$  and  $b_f$  that minimize the difference between  $Q_{obs}$  and  $Q_{sim}$ . The double entry Table 4 shows  $a_f$  and  $b_f$  estimated for each pair ports.

## 4 Discussion

In order to analyze the experimental results two dimensionless numbers have been evaluated: the Reynolds number and the Forchheimer number.

Reynolds number is defined as the ratio of inertial forces to viscous forces:

$$Re = \frac{\rho \bar{v} D_h}{\mu} \quad (15)$$

Where  $\bar{v}$  represents the average velocity evaluated on the active path and  $D_h$  represents the characteristic dimension. For fracture having small aperture respect to its

## Bench scale laboratory tests

C. Cherubini et al.

Title Page

Abstract

Introduction

Conclusions

References

Tables

Figures

◀

▶

◀

▶

Back

Close

Full Screen / Esc

Printer-friendly Version

Interactive Discussion



height, the characteristic dimension radius is equal to  $D_h = w/2$ . Assuming that the average specific discharge is equal to  $\bar{q} = \bar{v} \cdot w$  the Reynolds number becomes:

$$Re = \frac{\rho}{2\mu} \bar{q} \quad (16)$$

The Forchheimer number is the ratio of the non linear and linear pressure loss:

$$Fo = \frac{k\beta\rho\bar{v}}{\mu} \quad (17)$$

According to Eq. (8) the Forchheimer number can be reformulated as:

$$Fo = \frac{b_f \cdot \bar{q}}{a_f} \quad (18)$$

According to Zeng and Grigg (2006) the Forchheimer number is recommended as a criterion for identifying non-Darcy flow because it has the advantage of clear meaning. It equals the ratio of pressure drop caused by liquid-solid interactions to that by viscous resistance and it is directly related to the non-Darcy effect. Inertial effects dominate over viscous effects at the critical Forchheimer number ( $Fo > 1$ ) (Ruth and Ma, 1992).

Reynolds number instead is a dimensionless number that indicates when microscopic inertial effects become important. It is inappropriate on the macroscopic level because microscopic inertial effects do not directly lead to macroscopic inertial effects. In fact, high microscopic Reynolds number does not necessarily imply non-Darcian flow. Instead  $Fo$  indicates precisely the onset of non-Darcian flow (Ruth and Ma, 1992): it accounts for both velocity ( $v$ ) and structure of the medium because  $\beta$  is structure dependent. The term  $\beta$  inherently contains information on the tortuosity of the flow paths that leads to changes in the microscopic inertial terms. In fact, if the structure of the medium is such that microscopic inertial effects are rare, then  $\beta$  will be small and  $Fo$  will remain small until  $v$  (i.e.  $Re$ ) is large. Instead, both  $\beta$  and  $Fo$  will be large if the structure of the medium is such that microscopic inertial effects can be expected.

## Bench scale laboratory tests

C. Cherubini et al.

Title Page

Abstract

Introduction

Conclusions

References

Tables

Figures

◀

▶

◀

▶

Back

Close

Full Screen / Esc

Printer-friendly Version

Interactive Discussion



In the Fig. 8 the relationship between  $Re$  and  $Fo$  is graphed for each set of experiments. Under different ports configurations the Reynolds numbers are in the range 20–350 whereas the Forchheimer numbers are in the range 0.1–3.9.

The results showed in Fig. 8 are consistent with the previous considerations. For example even if the paths (1–4 and 4–6) reach relatively high values of  $Re$  they present values of  $Fo$  lower than unity.

The slope of the straight lines represents the ratio between  $Re$  and  $Fo$  that is equal to the ratio of their respective characteristic dimensions:

$$\zeta = \frac{D_h}{k\beta} \quad (19)$$

This dimensionless group  $\zeta$  is characteristic of the flow path. Relatively high values of this parameter correspond to a more linear flow behavior because the inertial effects dominate viscous ones at higher Reynolds numbers. Therefore it permits to distinguish a different behavior of the experiments carried out varying configurations of ports.

For each path the equivalent aperture  $w_{eq}$  has been estimated from the linear term assuming valid the cubic law:

$$w_{eq} = \sqrt[3]{\frac{\mu}{\rho g} \frac{12}{a_f}} \quad (20)$$

This term has been compared with the average measured aperture of each path  $w$  (Fig. 9). Though  $w_{eq}$  underestimates  $w$ , they are of the same order of magnitude.

A power law has been observed between the terms  $a$  and  $b$  (Fig. 10):

$$b = 0.9145 \cdot a^{2.6533} \quad (21)$$

This correlation between inertial and viscous coefficient is customary used in petroleum production engineering in order to predict high velocity well performance. Geertsma

## Bench scale laboratory tests

C. Cherubini et al.

Title Page

Abstract

Introduction

Conclusions

References

Tables

Figures

◀

▶

◀

▶

Back

Close

Full Screen / Esc

Printer-friendly Version

Interactive Discussion



(1974) and Skjetne et al. (1999) Found similar relationship for high velocity flow in porous media and fractures.

Zimmerman (1996) analyzed flow in two-dimensional rough walled rock fractures and individuated a factor equal to the ratio of the cubes of  $w_{eq}$  and  $w$  that reflects the tortuosity induced into the streamlines by the obstacles.

In the case of a single rock fracture this factor depends only on the planform of the asperity region. Whereas in the case study it depends on several parameters such as roughness, the areas where the rock faces are in contact with each other, fracture intersection, position and shape of the inlet and outlet ports:

$$\tau = \frac{w_{eq}^3}{w^3} \quad (22)$$

This parameter measures how much each path deviates from the parallel plate model.

The pressure drops depend by the morphology of the fracture wall surfaces and on the tortuosity of the flow paths. Significant head losses may be envisaged to occur adjacent to sharp corners of fracture where sudden change of aperture occurs (Javadi et al., 2010).

Figures 11 and 12 show the  $\tau - b$  and  $\tau - a$  relationships, respectively.  $\tau$  results correlated with  $b$  and  $a$  by means of a power function.

## 5 Conclusions

In this paper non-linear fluid flow through rock fractures was studied by means of laboratory tests and numerical modeling.

The Forchheimer equation has proved to explain reasonably the relationship between flow rate and pressure drop, which depicts a strong inertial regime where the viscous and inertial pressure drop are controlled, respectively by  $\nu$  and  $\nu^2$  term.

The equivalent linear and non linear terms of Forchheimer's law have been estimated by numerical modeling.

**Bench scale  
laboratory tests**

C. Cherubini et al.

Title Page

Abstract

Introduction

Conclusions

References

Tables

Figures

◀

▶

◀

▶

Back

Close

Full Screen / Esc

Printer-friendly Version

Interactive Discussion



The equivalent aperture of each flow path is determined assuming valid the cubic law. Though it underestimates the mean measured aperture it keeps its same order of magnitude.

A tortuosity factor  $\tau$  has been determined as the ratio of the cube of the equivalent aperture and the cube of the mean measured aperture. This factor measures how the flow path deviates from the parallel plate model. In other words it measures the effects of different factors such as roughness, the contact area between fracture surfaces, fracture intersections and the position and the form of the inlet and outlet ports.

A power law between the Forchheimer terms and  $\tau$  has been detected. In complex fracture networks the tortuosity factor plays an important role in fluid flow dynamics.

*Acknowledgements.* The authors would like to acknowledge the Editor Guadagnini for valuable advice.

## References

- Barrère, J.: Modélisation des écoulements de Stokes et Navier Stokes en milieu poreux, PhD thesis, Université de Bordeaux I, 1990.
- Basak, P. and Rajagopalan, S. P.: Effect of non-Darcy flow on computing seawater intrusion lengths, *J. Hydrol.*, 58, 83–87, 1982.
- Boutt, D. F., Grasselli, G., Fredrich, J. T., Cook, B. K., and Williams, J. R.: Trapping zones: The effect of fracture roughness on the directional anisotropy of fluid flow and colloid transport in a single fracture, *Geophys. Res. Lett.*, 33, L21402, doi:10.1029/2006GL027275, 2006.
- Brown, S.: Fluid flow through rock joints: The effect of surface roughness, *J. Geophys. Res.*, 92, 1337–1347, 1987.
- Brush, D. J. and Thomson, N. R.: Fluid flow in synthetic roughwalled fracture: Navier-Stokes, Stokes, and local cubic law simulations, *Water Resour. Res.*, 39, 1085, doi:10.1029/2002WR001346, 2003.
- Cakmak, A.: Analysis of nonlinear darcy – Forchheimer flows in porous media, Dissertation in mathematics, Texas Tech University, 74 pp., available at: [http://thinktech.lib.ttu.edu/ttu-ir/bitstream/handle/2346/8729/Cakmak\\_Adem\\_diss.pdf?sequence=1](http://thinktech.lib.ttu.edu/ttu-ir/bitstream/handle/2346/8729/Cakmak_Adem_diss.pdf?sequence=1), 2009.

### Bench scale laboratory tests

C. Cherubini et al.

Title Page

Abstract

Introduction

Conclusions

References

Tables

Figures

◀

▶

◀

▶

Back

Close

Full Screen / Esc

Printer-friendly Version

Interactive Discussion



- Cardenas, M. B., Slottke, D. T., Ketcham, R. A., and Sharp, J. M.: Navier-Stokes flow and transport simulations using real fractures shows heavy tailing due to eddies, *Geophys. Res. Lett.*, 34, L14404, doi:10.1029/2007GL030545, 2007.
- Cherubini, C., Giasi, C. I., and Pastore, N.: Fluid flow modeling of a coastal fractured karstic aquifer by means of a lumped parameter approach, *Environ. Earth Sci.*, online first: doi:10.1007/s12665-010-0851-5, ISSN:1866-6280, 2010.
- Chin, D. A., René, M. P., and Di Frenna, V. J.: Nonlinear flow in karst formations, *Ground Water*, 47, 669–674, doi:10.1111/j.1745-6584.2009.00574.x, 2009.
- Field, M. S.: Risk assessment methodology for karst aquifers, 2) Solute transport modeling, in: *Environmental Monitoring and Assessment*, Vol. 47, Kluwer Academic Publishers, 23–37, 1997.
- Forchheimer, P.: Wasserbewegung durch Boden, *Zeit. Ver. Deut. Ing.*, 45, 1781–1788, 1901.
- Geertsma, J.: Estimating the coefficient of inertial resistance in fluid flow through porous media, *SPE J.*, 14, 445–450, 1974.
- Geuzaine, C. and Remacke, J.: GMSH Reference Manual. A finite element mesh generator with built-in pre and pos-processing facilities, 252 pp., available at: <http://www.geuz.org/gmsh/doc/texinfo/gmsh.pdf>, 2009.
- Harbough, A. W.: MODFLOW-2005, the US geological survey modular ground-water model – the ground water flow process: US Geological Survey Techniques and Methods, 6-A16, available at: <http://pubs.usgs.gov/tm/2005/tm6A16/PDF.htm>, 2005.
- Hassanizadeh, S. and Gray, W.: High velocity flow in porous media, *Transport Porous Med.*, 2, 521–531, 1987.
- Ing, T. C. and Xiayan, N.: Coupled consolidation theory with non-Darcian flow, *Comput. Geotech.*, 29, 169–209, 2002.
- Izbash, S.: *O filtracii v Kropnozernstom Materiale*, Leningrad, 1931 (in Russian).
- Javadi, M., Sharifzadeh, M., and Shahriar, K.: A new geometrical model for nonlinear fluid flow through rough fractures, *J. Hydrol.*, 389, 18–30, 2010.
- Kohl, T., Evans, K. F., Hopkirk, R. J., Jung, R., and Rybach, L.: Observation and simulation of non-darcian flow transients in fractured rock, *Water Resour. Res.*, 33, 407–418, 1997.
- Kolditz, O.: Non-linear flow in fractured rock, *Int. J. Numer. Method. H.*, 11, 547–575, 2001.
- Lomize, G. M.: *Filtratsia v treshchinovatykh porodakh*, Seepage in Jointed Rocks, Gosudarstvennoe Energeticheskoe Izdatel'stvo, Moskva, Leningrad, 127 pp., 1951.

**Bench scale  
laboratory tests**

C. Cherubini et al.

Title Page

Abstract

Introduction

Conclusions

References

Tables

Figures

◀

▶

◀

▶

Back

Close

Full Screen / Esc

Printer-friendly Version

Interactive Discussion



---

**Bench scale  
laboratory tests**
C. Cherubini et al.

---

Title Page

Abstract

Introduction

Conclusions

References

Tables

Figures

◀

▶

◀

▶

Back

Close

Full Screen / Esc

Printer-friendly Version

Interactive Discussion



- Louis, C.: A study of groundwater flow in jointed rock and its influence on the stability of rock masses, Imperial College Mechanical Research Report 10, 90 pp., 1969.
- Mei, C. C. and Auriault, J. L.: The effect of weak inertia on flow through a porous medium, *J. Fluid Mech.*, 222, 647–663, 1991.
- 5 Moutsopoulos, K. N., Papaspyros, I., and Tsihrintzis, V.: A experimental investigation of inertial flow processes in porous media, *J. Hydrol.*, 374, 242–254, 2009.
- National Research Council: *Rock Fractures and Fluid Flow: Contemporary Understanding and Application*, National Academy Press, Washington, DC, 551 pp., available at: <http://www.nap.edu/openbook.php?isbn=0309049962>, 1996.
- 10 Qian, J., Zhan, H., Zhao, W., and Sun, F.: Experimental study of turbulent unconfined groundwater flow in a single fracture, *J. Hydrol.*, 311, 134–142, 2005.
- Qian, J. Z., Zhan, H. B., Luo, S. H., and Zhao, W. D.: Experimental evidence of scale dependent hydraulic conductivity for fully developed turbulent flow in a single fracture, *J. Hydrol.*, 339, 206–215, 2007.
- 15 Qian, J., Zhan, H., Chen, Z., and Ye, H.: Experimental study of solute transport under non-Darcian flow in a single fracture, *J. Hydrol.*, 399, 246–254, 2011.
- Ruth, D. W. and Ma, H.: *On the derivation of the Forchheimer equation by means of the averaging theorem*, *Transport in Porous Media*, 7, 255–264, Kluwer Academic Publishers, 1992.
- 20 Sisavath, S., Al-Yaarubi, C., and Zimmermann, R. W.: A simple model for deviates from the cubic law for a fracture undergoing dilation or closure, *Pure Appl. Geophys.*, 160, 1009–1022, 2003.
- Skjetne, E.: *High-velocity flow in porous media, analytical, numerical and experimental studies*, Doctoral Thesis at Departement of Petroleum Engineering and Applied Geophysics, Faculty of Applied Earth Sciences and Metallurgy, Norwegian University of Science and Technology, 1995.
- 25 Skjetne, E., Klov, T., and Gudmundsson, J. S.: Experiments and modeling of high-velocity pressure loss in sandstone fractures, SPE paper 56414 presented at the 1999 Annual Technical Conference and Exhibition in Houston, available at: <http://www.onepetro.org/mslib/servlet/onepetropreview?id=00056414>, 1999.
- 30 Vinciguerra, S. and Barnabé, Y.: *Rock Physics and Natural Hazards*, Birkhauser Verlag AG, Basel, Boston, Berlin, 429 pp., 2009.
- Wen, Z., Huag, G., and Zhan, H.: Non-Darcian flow in a single confined vertical fracture toward a well, *J. Hydrol.*, 330, 698–708, 2006.

Wen, Z., Huag, G., and Zhan, H.: An analytical solution for non-Darcian flow in a confined aquifer using the power law function, *Adv. Water Resour.*, 31, 44–55, 2008.

Witherspoon, P. A., Wang, J. S., Iway, K., and Gale, J. E.: Validity of cubic law for fluid flow in a deformable rock fracture, *Water Resour. Res.*, 16, 1016–1024, 1980.

5 Zeng, Z. and Grigg, R.: A criterion for non-Darcy flow in porous media, *Transport Porous Med.*, 63, 57–69, 2006.

Zimmermann, R. W. and Bodvarsson, G. S.: Hydraulic conductivity of rock fractures, *Transport Porous Med.*, 23, 1–30, 1996.

10 Zimmermann, R. W., Al-Yaarubi, A. H., Pain, C. C., and Grattoni, C. A.: Non-linear regimes of fluid flow in rock fractures, *Int. J. Rock Mech Min.*, 41, 163–169, 2004.

# HESSD

9, 5575–5609, 2012

## Bench scale laboratory tests

C. Cherubini et al.

Title Page

Abstract

Introduction

Conclusions

References

Tables

Figures

⏪

⏩

◀

▶

Back

Close

Full Screen / Esc

Printer-friendly Version

Interactive Discussion



**Bench scale  
laboratory tests**

C. Cherubini et al.

Title Page

Abstract

Introduction

Conclusions

References

Tables

Figures

I◀

▶I

◀

▶

Back

Close

Full Screen / Esc

Printer-friendly Version

Interactive Discussion

**Table 1.** Properties of the limestone block.

Bulk density ( $\text{gcm}^{-2}$ )	2.21
Porosity (%)	0.20
Moisture content (%)	2.44
Hydraulic conductivity ( $\text{ms}^{-1}$ )	1.63e-8

## Bench scale laboratory tests

C. Cherubini et al.

**Table 2.** Characteristic parameters of the discontinuities.

Fracture number	Mean aperture $b_m$ (mm)	Aperture range (mm)	Roughness $\varepsilon$ (mm)	Length (mm)	Fractal dimension $D$
1	1.496	0.811 ÷ 2.907	0.180	119	2.331
2	1.069	0.541 ÷ 1.977	0.187	88	2.292
3	1.076	0.573 ÷ 2.784	0.187	172	2.251
4	1.100	0.271 ÷ 3.900	0.101	171	2.314
5	1.040	0.811 ÷ 2.194	0.181	141	2.250
6	0.917	0.272 ÷ 1.794	0.141	107	2.241
7	0.906	0.540 ÷ 1.510	0.010	69	2.303
8	1.484	0.540 ÷ 3.097	0.150	62	2.321
9	0.703	0.540 ÷ 3.577	0.450	155	2.204
10	0.875	0.810 ÷ 1.300	0.063	65	2.202
11	1.075	0.270 ÷ 2.901	0.152	78	2.263
12	0.921	0.544 ÷ 1.912	0.135	246	2.244
13	1.130	0.541 ÷ 1.9097	0.096	258	2.277
14	1.576	0.344 ÷ 3.050	0.222	143	2.254

Title Page

Abstract

Introduction

Conclusions

References

Tables

Figures

◀

▶

◀

▶

Back

Close

Full Screen / Esc

Printer-friendly Version

Interactive Discussion



## Bench scale laboratory tests

C. Cherubini et al.

**Table 3.** Double entry table. Upper and lower triangular matrix represents the linear coefficient (*A*) and the non linear coefficient (*B*), respectively obtained for each pair of the ports.

	1	2	3	4	5	6	7
1	–	1.54e4	4.16e4	1.77e4	3.06e4	1.63e4	1.47e5
2	<b>1.53e9</b>	–	3.71e4	2.81e4	4.11e4	2.42e4	2.06e5
3	<b>2.79e9</b>	<b>3.75e9</b>	–	5.78e4	7.32e4	5.62e4	2.50e5
4	<b>7.22e8</b>	<b>3.00e9</b>	<b>3.94e9</b>	–	3.42e4	1.45e4	1.64e5
5	<b>4.01e9</b>	<b>6.61e9</b>	<b>7.80e9</b>	<b>3.58e9</b>	–	2.90e4	1.83e5
6	<b>1.11Ee9</b>	<b>2.73e9</b>	<b>4.22e9</b>	<b>9.18e8</b>	<b>6.71e9</b>	–	2.28e5
7	<b>3.22e11</b>	<b>2.66e11</b>	<b>2.66e11</b>	<b>2.79e11</b>	<b>2.95e11</b>	<b>2.97e11</b>	–

Title Page

Abstract

Introduction

Conclusions

References

Tables

Figures

◀

▶

◀

▶

Back

Close

Full Screen / Esc

Printer-friendly Version

Interactive Discussion



## Bench scale laboratory tests

C. Cherubini et al.

**Table 4.** Double entry table. Upper and lower triangular matrix represents the linear coefficient ( $a_i$ ) and the non linear coefficient ( $b_i$ ), respectively obtained for each pair of the ports.

	1	2	3	4	5	6	7
1	–	2.96e3	6.34e3	2.64e3	5.29e3	3.11e3	3.02e4
2	<b>1.94e7</b>	–	8.04e3	3.83e3	6.30e3	3.88e3	2.99e4
3	<b>5.77e7</b>	<b>1.02e8</b>	–	5.86e3	8.43e3	6.97e3	3.00e4
4	<b>9.32e6</b>	<b>2.91e7</b>	<b>6.33e7</b>	–	6.10e03	2.97e3	2.06e4
5	<b>5.69e7</b>	<b>8.34e7</b>	<b>1.42e8</b>	<b>7.15e7</b>	–	1.33e4	2.62e4
6	<b>1.66e7</b>	<b>3.39e7</b>	<b>8.92e7</b>	<b>1.51e7</b>	<b>3.80e8</b>	–	3.91e4
7	<b>4.97e9</b>	<b>3.91e9</b>	<b>3.74e9</b>	<b>2.47e9</b>	<b>3.53e9</b>	<b>5.67e9</b>	–

Title Page

Abstract

Introduction

Conclusions

References

Tables

Figures

◀

▶

◀

▶

Back

Close

Full Screen / Esc

Printer-friendly Version

Interactive Discussion



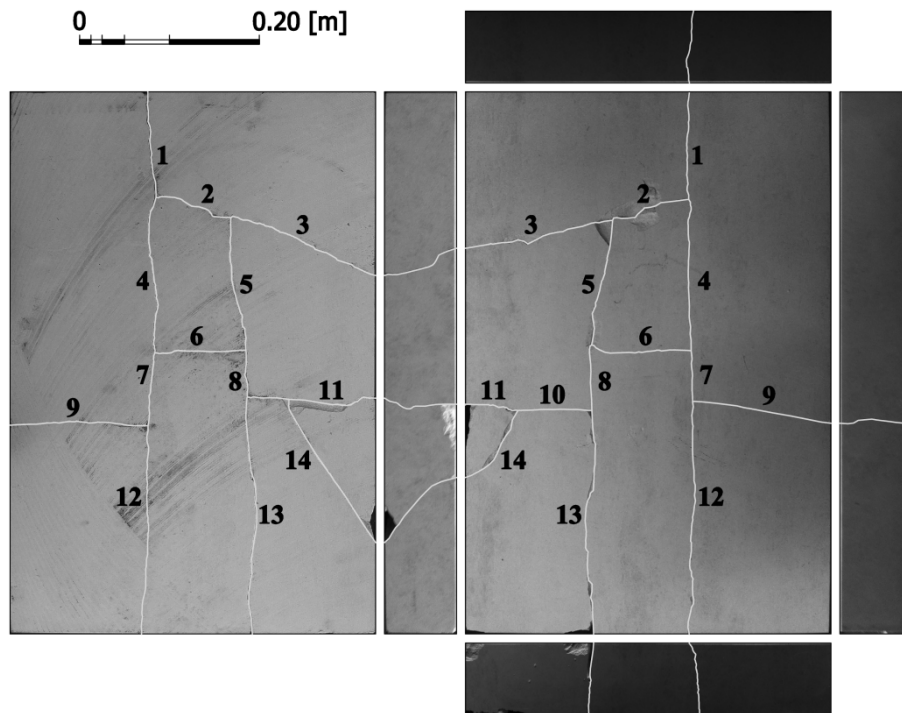


**Fig. 1.** Block sample rectified images ( $0.6 \times 0.4 \times 0.08 \text{ m}^3$ ). White traces indicate the median profiles.

**Bench scale  
laboratory tests**

C. Cherubini et al.

Title Page

Abstract Introduction

Conclusions References

Tables Figures

◀ ▶

◀ ▶

Back Close

Full Screen / Esc

Printer-friendly Version

Interactive Discussion



Bench scale  
laboratory tests

C. Cherubini et al.

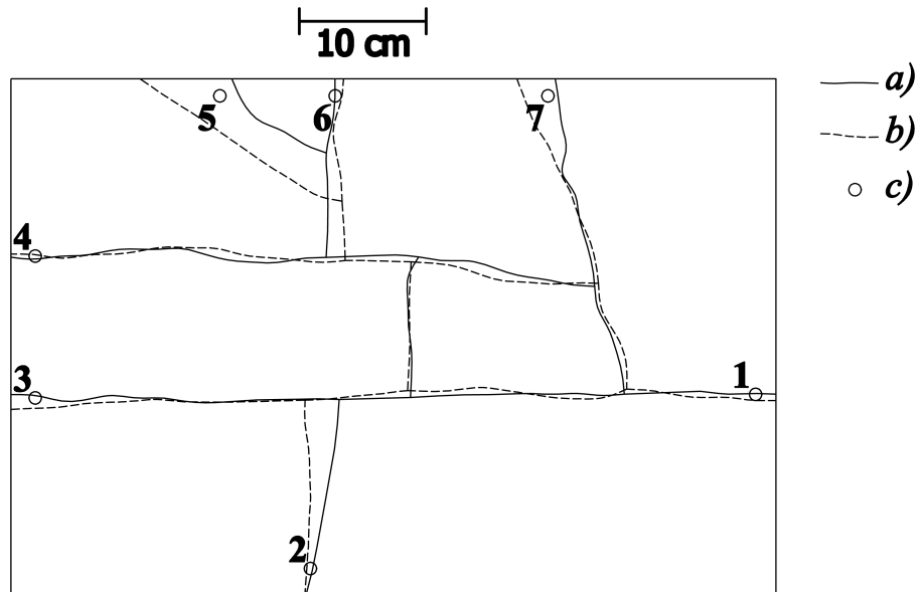


**Fig. 2.** Localization of the ports on the top surface of block, (a) top fracture traces (b) bottom fracture traces (c) ports.

[Title Page](#)[Abstract](#)[Introduction](#)[Conclusions](#)[References](#)[Tables](#)[Figures](#)[I◀](#)[▶I](#)[◀](#)[▶](#)[Back](#)[Close](#)[Full Screen / Esc](#)[Printer-friendly Version](#)[Interactive Discussion](#)

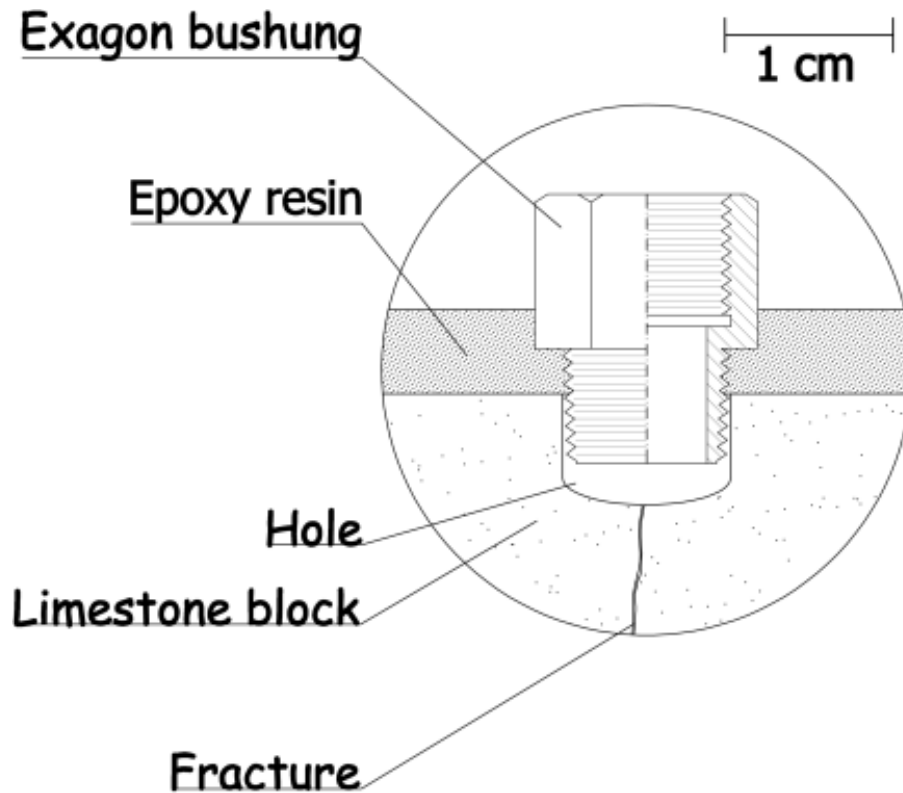


**Fig. 3.** Illustration of a “port” construction details.

Title Page

Abstract

Introduction

Conclusions

References

Tables

Figures

◀

▶

◀

▶

Back

Close

Full Screen / Esc

Printer-friendly Version

Interactive Discussion



## Bench scale laboratory tests

C. Cherubini et al.

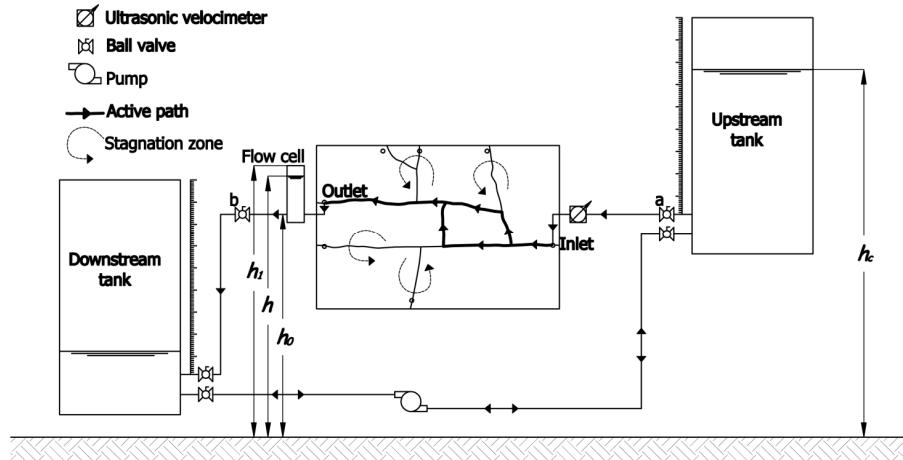


**Fig. 4.** Schematic diagram of the experimental setup (picture is not to scale).

Title Page	
Abstract	Introduction
Conclusions	References
Tables	Figures
◀	▶
◀	▶
Back	Close
Full Screen / Esc	
Printer-friendly Version	
Interactive Discussion	



## Bench scale laboratory tests

C. Cherubini et al.

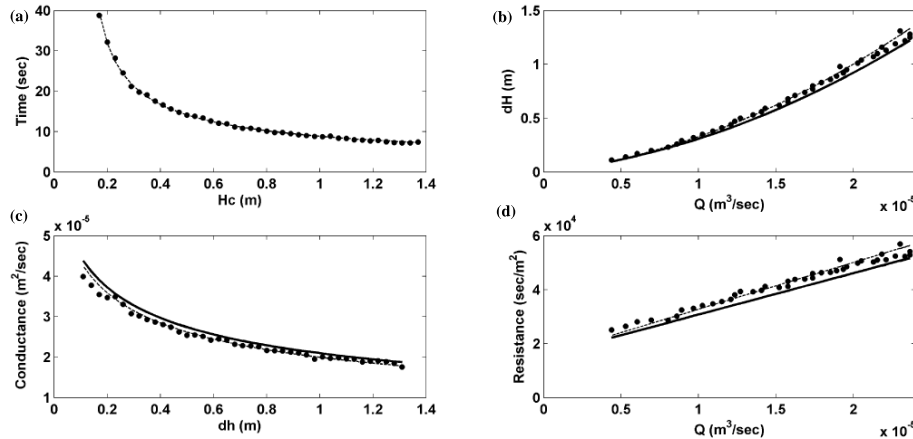


**Fig. 5.** Experimental results obtained for 1–2 configuration ports. **(a)** Control head  $H_c$  vs. time. **(b)** average flow rate  $Q$  vs. difference head evaluated as  $dh = H_c + (h_0 + h_1)/2$  **(c)** difference head vs. conductance term evaluated as Eq. (13) **(d)** average flow rate vs. resistance term evaluated as the inverse of conductance. Dots represents the experimental values, dashed line represents the fitting of experimental values, marked line represents the functions without the effect of circuit ( $C = 0$ ).

Title Page

Abstract

Introduction

Conclusions

References

Tables

Figures

◀

▶

◀

▶

Back

Close

Full Screen / Esc

Printer-friendly Version

Interactive Discussion



Bench scale  
laboratory tests

C. Cherubini et al.

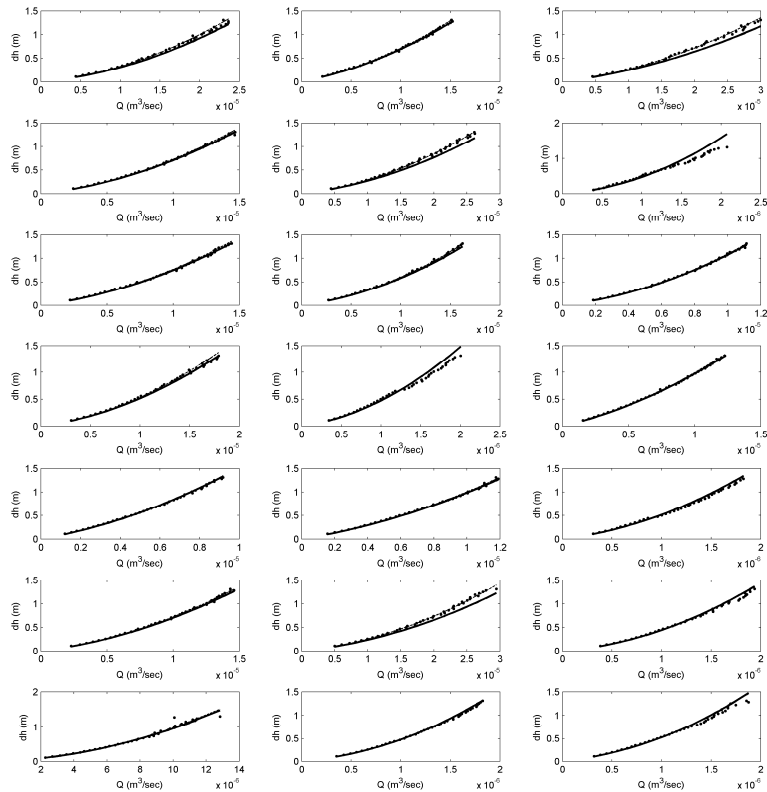


**Fig. 6.** Flow rate  $Q$  vs. hydraulic head difference  $dh$  for all the experiments. Dots represents the experimental values, dashed line represents the fitting of experimental values, marked line represents the relationship without the effect of circuit ( $C = 0$ ).

Title Page

Abstract

Introduction

Conclusions

References

Tables

Figures

◀

▶

◀

▶

Back

Close

Full Screen / Esc

Printer-friendly Version

Interactive Discussion



**Bench scale  
laboratory tests**

C. Cherubini et al.

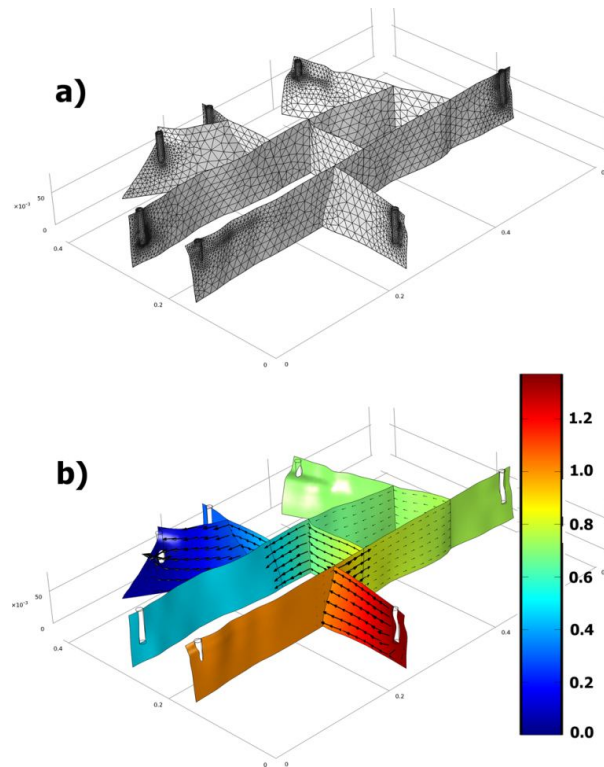


**Fig. 7.** (a) Finite element mesh of numerical model (b) a result of a simulation, color scale indicates the hydraulic head, black arrow represents the specific discharge.

[Title Page](#)[Abstract](#)[Introduction](#)[Conclusions](#)[References](#)[Tables](#)[Figures](#)[◀](#)[▶](#)[◀](#)[▶](#)[Back](#)[Close](#)[Full Screen / Esc](#)[Printer-friendly Version](#)[Interactive Discussion](#)





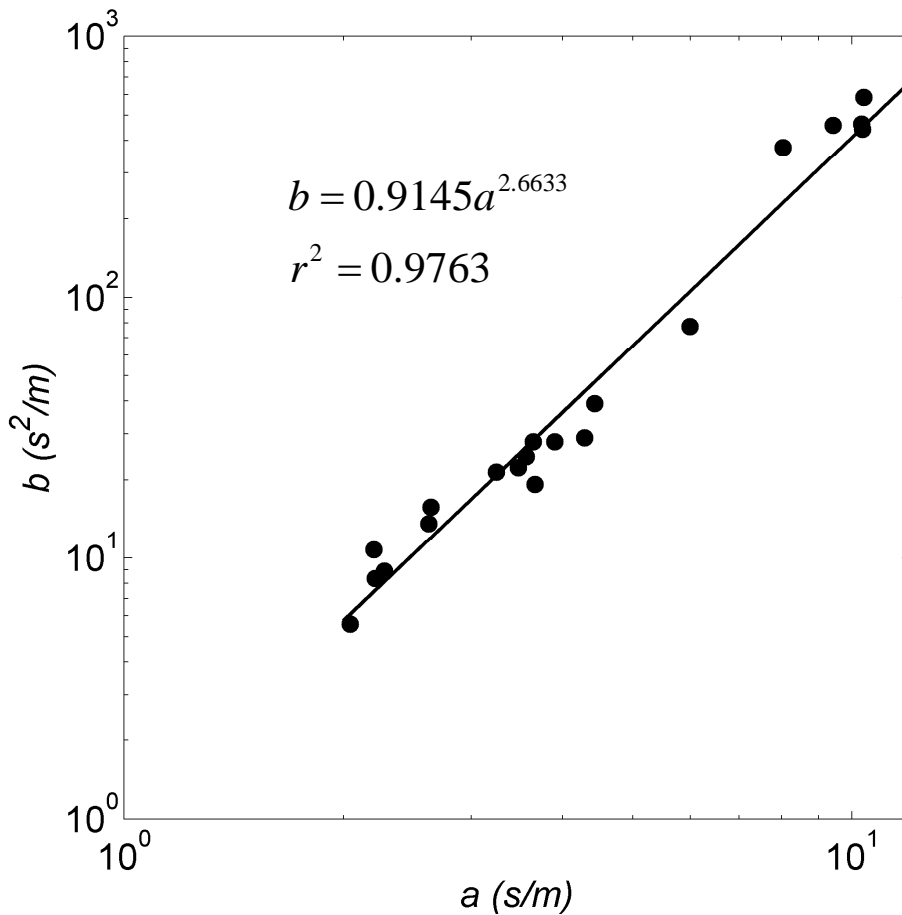


Fig. 10. Linear term  $a$  vs. non linear term  $b$ .

**Bench scale laboratory tests**

C. Cherubini et al.

Title Page

Abstract Introduction

Conclusions References

Tables Figures

◀ ▶

◀ ▶

Back Close

Full Screen / Esc

Printer-friendly Version

Interactive Discussion



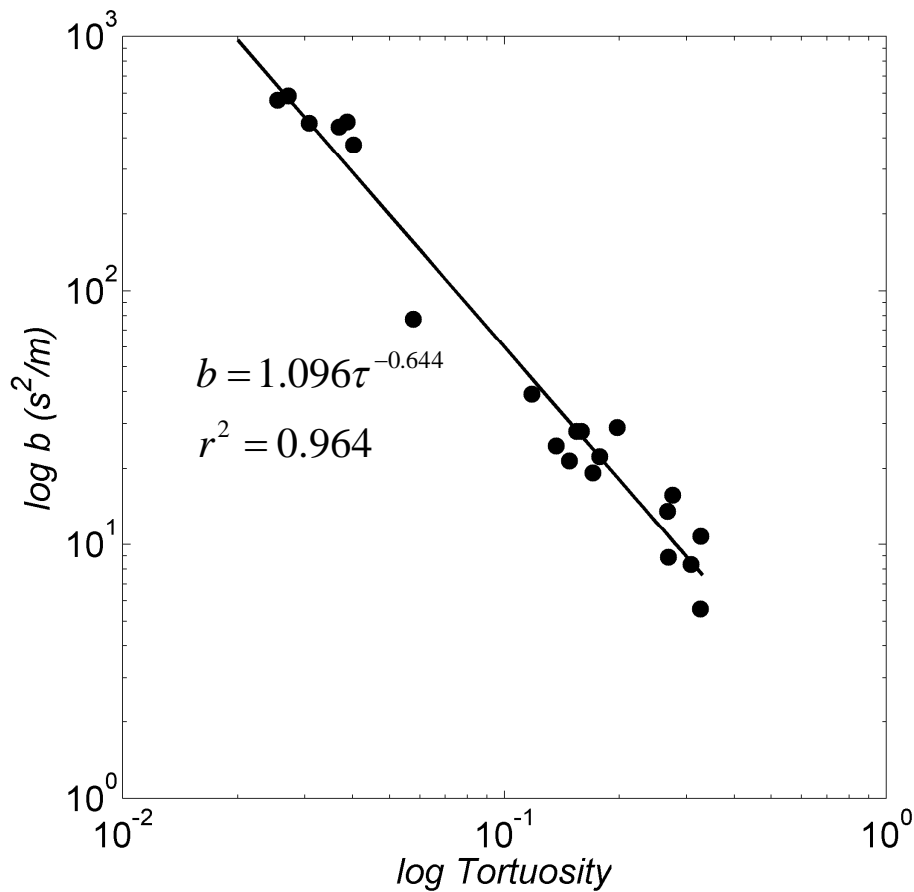


Fig. 11. Tortuosity factor  $\tau$  vs. non linear term  $b$ .

**Bench scale laboratory tests**

C. Cherubini et al.

Title Page

Abstract Introduction

Conclusions References

Tables Figures

◀ ▶

◀ ▶

Back Close

Full Screen / Esc

Printer-friendly Version

Interactive Discussion



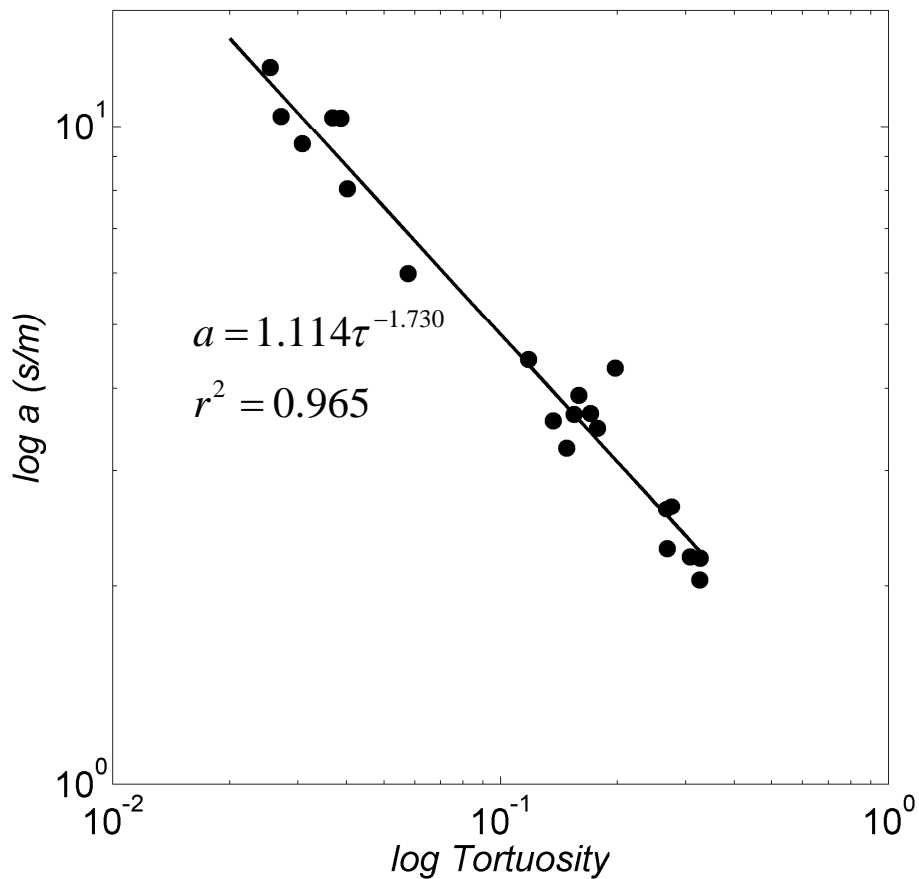


Fig. 12. Tortuosity factor  $\tau$  vs. linear term  $a$ .

## Bench scale laboratory tests

C. Cherubini et al.

Title Page	
Abstract	Introduction
Conclusions	References
Tables	Figures
◀	▶
◀	▶
Back	Close
Full Screen / Esc	
Printer-friendly Version	
Interactive Discussion	

